Biochemical and Biophysical Research Communications 453 (2014) 493–497

Contents lists available at ScienceDirect

Biochemical and Biophysical Research Communications

journal homepage: www.elsevier.com/locate/ybbrc

Crystal structure of archaeal homolog of proteasome-assembly chaperone PbaA

Arunima Sikdar [a,b,c], Tadashi Satoh [c,d], Masato Kawasaki [e], Koichi Kato [a,b,c,*]

[a] School of Physical Science, The Graduate University for Advanced Studies, 5-1 Higashiyama, Myodaiji, Okazaki, Aichi 444-8787, Japan
[b] Okazaki Institute for Integrative Bioscience and Institute for Molecular Science, National Institutes of Natural Sciences, 5-1 Higashiyama, Myodaiji, Okazaki, Aichi 444-8787, Japan
[c] Graduate School of Pharmaceutical Sciences, Nagoya City University, 3-1 Tanabe-dori, Mizuho-ku, Nagoya 467-8603, Japan
[d] JST, PRESTO, 3-1 Tanabe-dori, Mizuho-ku, Nagoya 467-8603, Japan
[e] Structural Biology Research Center, Photon Factory, Institute of Materials Structure Science, High Energy Accelerator Research Organization (KEK), Oho 1-1, Tsukuba, Ibaraki 305-0801, Japan

ARTICLE INFO

Article history:
Received 22 September 2014
Available online 5 October 2014

Keywords:
Archaea
Proteasome activator
Proteasome-assembly chaperone
Protein degradation

ABSTRACT

Formation of the eukaryotic proteasome is not a spontaneous process but a highly ordered process assisted by several assembly chaperones. In contrast, archaeal proteasome subunits can spontaneously assemble into an active form. Recent bioinformatic analysis identified the proteasome-assembly chaperone-like proteins, PbaA and PbaB, in archaea. Our previous study showed that the PbaB homotetramer functions as a proteasome activator through its tentacle-like C-terminal segments. However, a functional role of the other homolog PbaA has remained elusive. Here we determined the 2.25-Å resolution structure of PbaA, illustrating its disparate tertiary and quaternary structures compared with PbaB. PbaA forms a homopentamer in which the C-terminal segments, with a putative proteasome-activating motif, are packed against the core. These findings offer deeper insights into the molecular evolution relationships between the proteasome-assembly chaperones and the proteasome activators.

1. Introduction

Protein degradation in cells is essential for the homeostasis of all living organisms. In this system, majority of intracellular proteins are degraded by the ubiquitin–proteasome system in an ATP-dependent manner [1–3]. The proteasome forms a huge multi-subunit complex and is composed of a catalytic core particle (also called 20S proteasome) and one or two 19S regulatory particles (19S proteasome). The 20S proteasome consists of seven homologous α subunits and seven homologous β subunits that are assembled into a cylindrical structure consisting of four hetero-heptameric rings [4,5]. The resulting $\alpha_{1-7}\beta_{1-7}\beta_{1-7}\alpha_{1-7}$ barrel-like architecture is characterized by a twofold rotational symmetry, with each half containing an outer ring of seven α subunits and an inner ring of seven β subunits. While the two β rings contact each other to form the catalytic chamber of the 20S core particle, each α ring caps the chamber with a central channel gated by regulatory protein complexes termed proteasome activators. The 19S proteasome, a major eukaryotic proteasome activator composed of at least 19 subunits, is responsible for capturing the ubiquitin-tagged substrate, activating the 20S proteasome through gate opening, and eliminating the ubiquitin chain from the substrate [1–3]. The 19S proteasomes dock onto the 20S proteasome through their C-terminal tails containing a hydrophobic-Tyr-unspecified residue (HbYX) motif of three ATPase subunits, thereby facilitating gate opening [6–10].

Accumulated evidence has recently revealed that formation of the eukaryotic proteasome does not occur due to spontaneous self-organization but results from highly ordered processes mediated by several assembly chaperones that transiently associate with immature proteasome assembly intermediates [11,12]. Formation of the 20S proteasome is assisted by five assembly chaperones, i.e., PAC1, PAC2, PAC3, PAC4, and UMP1, whereas assembly of 19S proteasome is also assisted by five chaperones, i.e., Hsm3, Nas2, Nas6, Rpn14, and Adc17. To date, the 3D structures have been determined for several assembly chaperones [13–20]. These data have provided the structural basis of specific interactions between the proteasome-assembly chaperones and proteasomal subunits. Yeast orthologs of PAC1 and PAC2 (termed Pba1 and Pba2, respectively) possess the C-terminal HbYX proteasome-binding motifs, which, however, are not capable of stimulating the proteasome activation

* Corresponding author at: Okazaki Institute for Integrative Bioscience and Institute for Molecular Science, National Institutes of Natural Sciences, 5-1 Higashiyama, Myodaiji, Okazaki, Aichi 444-8787, Japan. Fax: +81 564 59 5224.
E-mail address: kkatonmr@ims.ac.jp (K. Kato).

http://dx.doi.org/10.1016/j.bbrc.2014.09.114
0006-291X/

Table 1
Data collection and refinement statistics for PbaA.

	Native	Edge	High remote
Crystallographic data			
Space group	$C222_1$	$C222_1$	$C222_1$
Unit cell $a/b/c$ (Å)	111.4/155.2/172.0	111.1/155.2/172.5	111.1/155.3/172.5
Data processing statistics			
Beam line	PF-AR NW12A	NSRRC 13B1	NSRRC 13B1
Wavelength (Å)	0.9792	1.0721	1.0539
Resolution (Å)	50–2.25 (2.29–2.25)	30–2.80 (2.90–2.80)	30–2.80 (2.90–2.80)
Total/unique reflections	523,885/71,040	268,062/37,188	266,899/37,188
Completeness (%)	99.9 (100.0)	100.0 (100.0)	99.9 (100.0)
R_{merge} (%)	8.4 (42.1)	11.6 (72.3)	11.3 (73.6)
I/σ (I)	40.1 (6.7)	18.6 (2.6)	19.1 (2.7)
Refinement statistics			
Resolution (Å)	40.0–2.25		
R_{cryst}/R_{free} (%)	19.6/22.0		
r.m.s. deviations from ideal			
Bond lengths (Å)	0.012		
Bond angles (°)	1.53		
Ramachandran plot (%)			
Favored	98.3		
Allowed	1.7		
Number of atoms			
Protein atoms (A/B/C/D/E)	1755/1772/1764/1764/1715		
Water molecules	308		
Average B factors (Å^2)			
Protein atoms	33.4/32.9/35.5/38.4/65.4		
Water molecules	34.1		

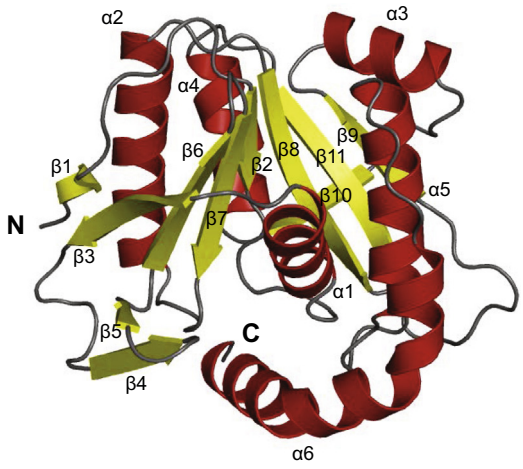

Fig. 1. Crystal structure of PbaA protomer. Ribbon model of the PbaA protomer. β-Strands, α-helices, and loops are shown in yellow, red, and gray, respectively. Positions of the N- and C-termini are indicated.

[20], whereas Nas2 masks the C-terminal proteasome-activating motif of a 19S proteasome subunit, Rpt5, during proteasome orchestration processes [18].

In contrast to eukaryotic proteasomes, archaeal 20S proteasome subunits are much less divergent and typically described as only a single form of each α- and β-subunit, which spontaneously assemble into four heteroheptameric rings *in vitro* [4]. Recent bioinformatic analysis has identified the PAC1-2 homologs PbaA and PbaB from archaeon *Methanococcus maripaludis* [21]. The archaeal homologs also share the C-terminal proteasome-binding HbYX motif [11,12]. However, it is enigmatic how the archaeal homologs are involved in proteasome assembly, which can proceed spontaneously *in vitro* and probably also in archaeal cells. Our recent study has revealed that the archaeon *Pyrococcus furiosus* PbaB acts as an ATP-independent proteasome activator [22]. Furthermore, the biochemical data showed that PbaA did not bind to the 20S proteasome despite its proteasome-binding HbYX motif. These findings raised questions as to why the HbYX motif-containing PbaA is not able to bind the proteasome and what is the functional role of this protein in archaeal cells. To address these issues, we herein performed a crystallographic study of *P. furiosus* PbaA.

2. Materials and methods

2.1. Protein expression, purification, and crystallization

Expression and purification of *P. furiosus* PbaA (PF0015, residues 1–242) was performed according to a method previously described [22]. The hexahistidine-tagged PbaA was purified using a Ni^{2+}-immobilized affinity column (Chelating Sepharose, GE Healthcare), anion exchange column (HiTrap Q HP), and gel-filtration column (HiLoad Superdex 200) from *Escherichia coli* soluble lysate. After the affinity chromatography, thrombin protease was used to remove the hexahistidine tag.

The purified PbaA protein was concentrated to 11.0 mg ml^{-1} in 50 mM Tris–HCl (pH 7.5) and used for crystallization. The crystallization screening and optimization experiments were performed by sitting-drop and hanging-drop vapor diffusion methods, respectively. The crystals of PbaA were obtained in a buffer containing 1.4 M sodium citrate tribasic and 0.1 M HEPES (pH 7.5) at 293 K for 3 days. To obtain the Pt-bound PbaA complex, the native crystal was soaked into the crystallization mother liquor buffer containing 5 mM $K_2Pt(NO_2)_4$ for 6 h using Heavy Atom Screen Pt kit (Hampton Research).

2.2. X-ray diffraction data collection and structure determination

Crystals were transferred into crystallization mother liquor and stored in liquid nitrogen. The native and anomalous datasets were collected using synchrotron radiation at AR-NW12A of the Photon Factory (PF, Japan) and 13B1 of the National Synchrotron Radiation Research Center (NSRRC, Taiwan). The native dataset was collected at wavelength of 0.9792 Å at PF, and the multi-wavelength

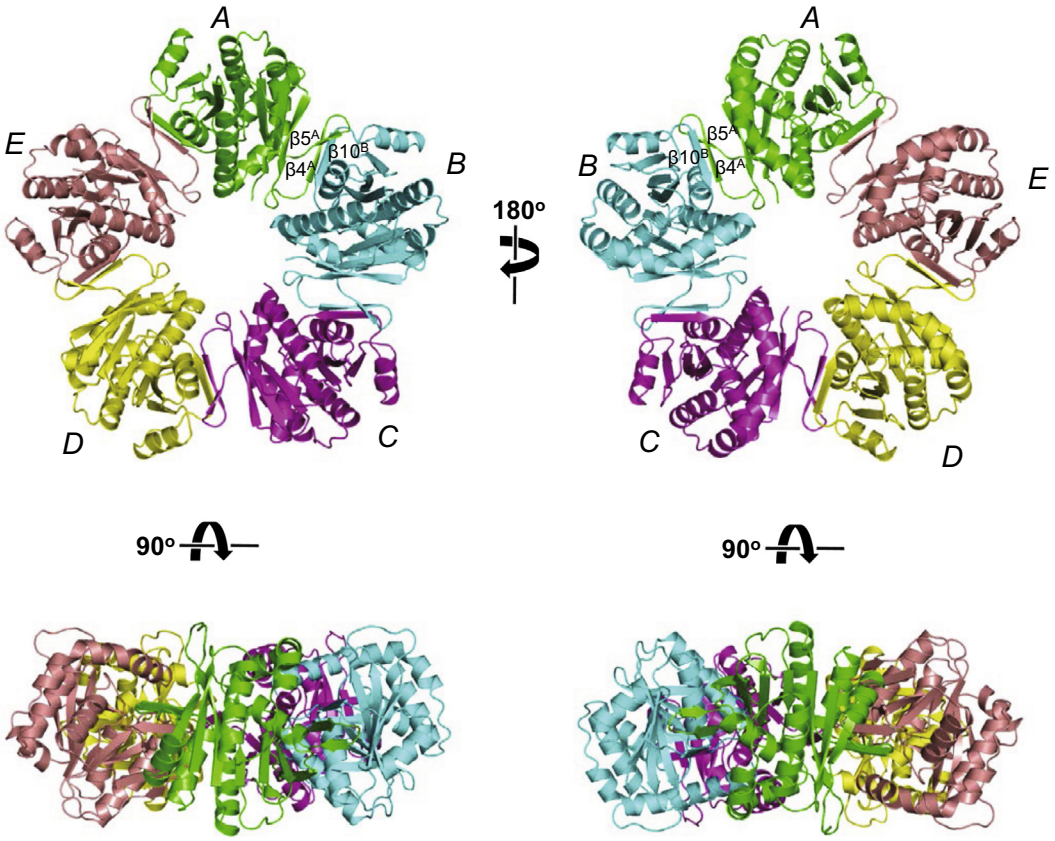

Fig. 2. PbaA forms a homopentamer. Ribbon models of the PbaA pentamer are shown on the left and right. The two structures are related by a rotation of 180° around a vertical axis (upper). Chains *A*, *B*, *C*, *D* and *E* are colored green, cyan, magenta, yellow, and pink, respectively. The two structures are also shown after 90° rotation around a horizontal axis in below. The β-hairpin (β4 and β5) makes an interface with β10 of the neighboring chain (β4/β5 of chain *A* and β10 of chain *B* are highlighted).

anomalous dispersion (MAD) datasets were collected at wavelengths of 1.0721 Å (*edge*) and 1.0539 Å (*high remote*) at NSRRC. All diffraction data were processed using HKL2000 [23]. The crystal parameters of native and $K_2Pt(NO_2)_4$-soaked PbaA are shown in Table 1.

The 2.80 Å-resolution crystal structure of PbaA was solved by the MAD method. The initial phase was determined using CRANK suite [24]. Because the Pt-soaked and native datasets were adequately isomorphous (Table 1), the phase information obtained from the MAD dataset could be transferred to the native dataset. After the density modification and phase extension to 2.25 Å using DM [25], the electron density map became unambiguous enough to be interpreted. The initial models were then built automatically using ARP/wARP [26]. Further manual model building into the electron density maps were conducted using COOT [27]. The refinement procedure was performed using REFMAC5 [28]. The stereochemical quality of the final model was validated using RAMPAGE [29]. The final refinement statistics are summarized in Table 1. Graphic figures were prepared using PyMOL (http://www.pymol.org/).

3. Results and discussion

3.1. Crystal structure of PbaA

We first tried to solve the crystal structure of *P. furiosus* PbaA by molecular replacement using the crystal structures of PbaA homologs, i.e., *P. furiosus* PbaB (PDB entry 3VR0) and Ta1441, a hypothetical protein from *Thermoplasma acidophilum*, (PDB entry 3GAA) as search models. However, we could not find a molecular replacement solution despite numerous trials using search models with various modifications, including homology modeling and potential loop truncations. We consequently performed heavy-atom derivatization experiments and successfully solved the 2.25-Å resolution crystal structure by the MAD method using the Pt^{2+}-bound crystal belonging to space group $C222_1$ with five molecules per asymmetric unit. The final model of PbaA has an R_{cryst} of 19.6% and R_{free} of 22.0% (Table 1).

In the crystal structure, N- and C-terminal residues consisting of Met1-Gly4 and Glu234-Leu242 are completely disordered. In addition, β6-β7 loop (residues Gly73-Asn76) in chain *E* gave no interpretable electron density. The overall chain *E* shows poor electron densities with high crystallographic *B* factor compared with those of chains *A*–*D* (Table 1, Supplementary Fig. 1). This is probably due to the subtle crystal contact around chain *E* (data not shown).

The crystal structure of PbaA showed a pentameric structure with the contact area (825–886 $Å^2$) buried through formation of the quaternary structure. Our previous analytical ultracentrifugation data also indicated that PbaA makes a stable pentamer in solution [22]. The overall structure of each PbaA protomer, which are essentially identical with a root mean square deviation (r.m.s.d.) of 0.17–0.26 Å for superimposed 221–226 Cα atoms, exhibits a three-layered αβα fold constituted from a central eight-stranded β-sheet (β1-β3-β6-β7-β2-β8-β11-β9) flanked by two α-helices (α2 and α4) and one β-strand (β10) on one side and four α-helices (α1, α3, α5, and α6) (Fig. 1). The protruding β4-β5 hairpin is responsible for the pentamerization through the formation of a three-stranded antiparallel β-sheet with β10 from the neighboring subunit (highlighted in Fig. 2). The C-terminal α6 helices showed high crystallographic *B* factors (Supplementary Fig. 1).

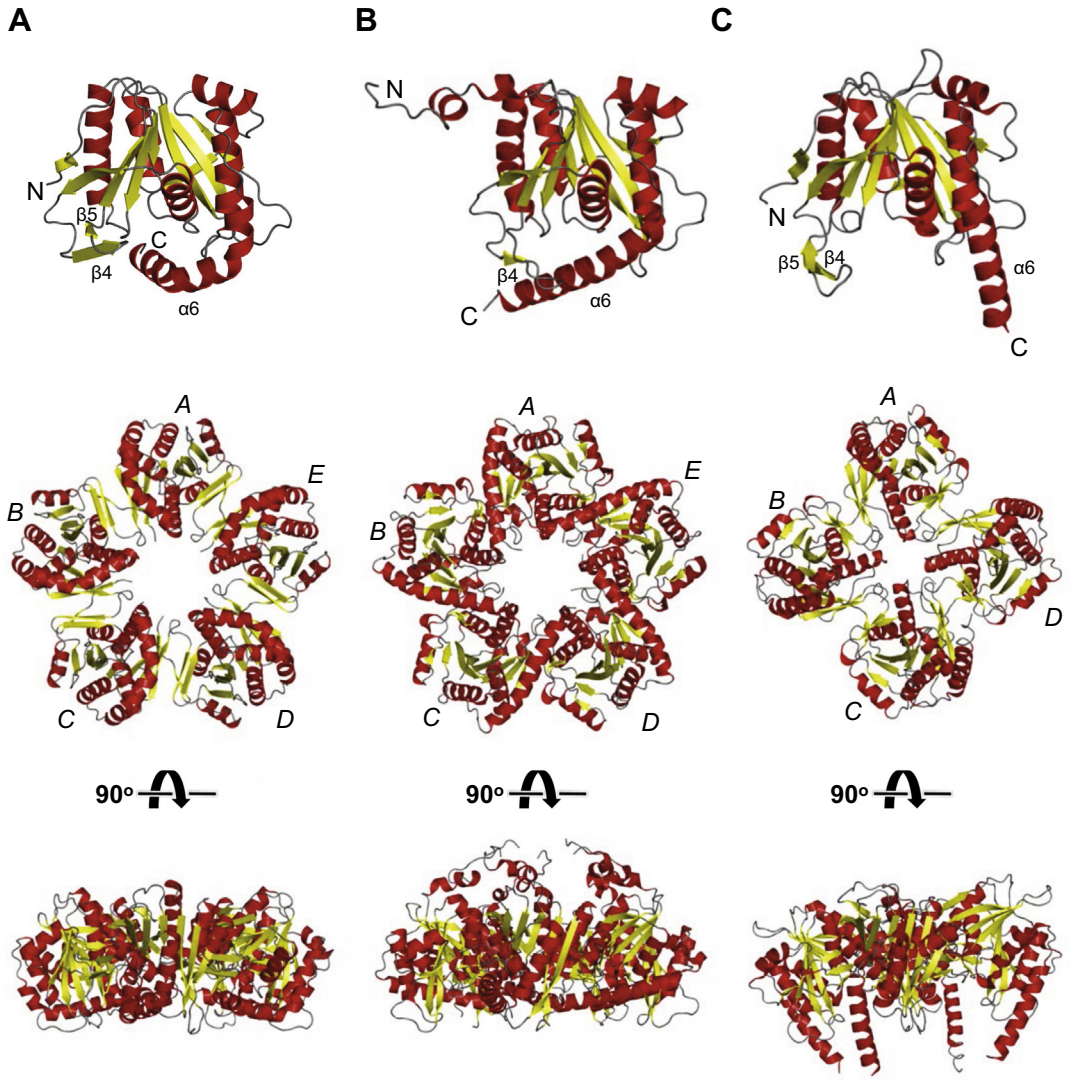

Fig. 3. Comparison of PbaA, Ta1441, and PbaB. Ribbon models of PbaA, Ta1441, and PbaB are shown in A, B and C, respectively. The secondary structures are colored as in Fig. 1. Their protomer structures are show in top. Their oligomer structures are shown in middle and bottom, which are rotated by 90° around a horizontal axis. The chain symbols are also indicated.

3.2. Structural comparison with other archaeal homologs of proteasome-assembly chaperone

The overall structure of the PbaA protomer is very similar to those of PbaB and Ta1441 (Fig. 3). The Ta1441 also forms a homopentamer in the crystal (PDB entry 3GAA). The PbaA can be superimposed with Ta1441 with r.m.s.d. values of 2.19 Å for 205 Cα atoms (as protomer, chain *A*) and 3.27 Å for 932 Cα atoms (as pentamer). PbaA and PbaB protomers can be superimposed with r.m.s.d. of 2.21 Å for 205 Cα atoms (chain *A*).

Despite the overall structural similarity of the protomers of these three proteins, significant conformational variations exist among them, which are associated with the differences in their quaternary structures and biological functions. The quaternary structure difference between PbaA and PbaB is ascribed to the local conformational variation around the β4 strand and consequent difference in subunit contact area, i.e., PbaA for 825–886 Å^2; PbaB for 1072–1184 Å^2 [22]. Although both PbaA and Ta1441 form a homopentameric structure, their β4 loop conformations are significantly different: Ta1441 lacks the β5 strand but makes a β-sheet with the adjoining molecule through its short β4 strand.

Most importantly, orientation of the C-terminal segment containing the potential proteasome-activating HbYX motif is remarkably different between pentameric PbaA/Ta1441 and tetrameric PbaB (Fig. 3). Although minor structural changes of α6 are observed between PbaA and Ta1441, their overall arrangement is almost consistent: the α6 helices are anchored inside the core. The α6 of PbaA is kinked so as to be accommodated on its own protomer core, whereas the C-terminal helix of Ta1441 is extended and in contact with a neighboring subunit, thereby forming a "star" shape (Fig. 3B). In contrast, the α6 helices of PbaB show tentacle-like structures that are projected from the core domain and extend in the same direction [22]. In the pentameric PbaA/Ta1441, the α6 helix is stabilized exclusively through hydrophobic interactions with the core (Supplementary Fig. 2A and B). A salt bridge between Glu216 and Arg182 observed in PbaA is not conserved in Ta1441. On the other hand, the protruding α6 helix of PbaB is stabilized through both hydrophobic and electrostatic interactions with Leu45/Ile215 and Lys219/Lys222 residues, respectively (Supplementary Fig. 2C). The charged residue pair, Lys219 and Glu249, is conserved among archaeal PbaB homologs. These structural features may explain the distinct 20S proteasome binding abilities of archaeal homologs of proteasome-assembly chaperone: PbaB but not PbaA could bind

the 20S proteasome, thereby functioning as a proteasome activator [22]. Previous proteomics analysis revealed that PbaA forms a stable complex with a hypothetical protein (PF0014) [30]. It is plausible that PbaA alone is in an inactive state, as demonstrated by the crystal structure but may become allosterically activated upon its complex formation with this binding partner so as to interact with the 20S proteasome through its C-terminal segments.

In summary, we determined the 2.25-Å resolution crystal structure of the archaeal homolog of the proteasome-assembly chaperone PbaA. Our crystallographic data revealed the distinct structural features of potential C-terminal proteasome-activating segments among archaeal Pba proteins. These findings not only offer insights into the molecular evolution relationships between the proteasome-assembly chaperones and the proteasome activators but also provide clues as to how scaffolds are designed to create distinct homooligomeric structures with homologous protomers.

Accession numbers

The coordinate and structural factor of the crystal structure of *P. furiosus* PbaA has been deposited in the Protein Data Bank under accession number, 3WZ2.

Acknowledgments

We thank Drs. Hisayoshi Makyio (KEK, Tsukuba, Japan) and Chiang Cheng-Hung (NSRRC, Hsinchu, Taiwan) for help with X-ray data collection. Diffraction datasets were collected at NSRRC using beamline 13B1 (Taiwan) and Photon Factory using AR-NW12A (Japan). We also thank Dr. Tsunehiro Mizushima and Mr. Kentaro Kumoi for their contributions during the early stage of this study. The strain *Pyrococcus furiosus* (JCM 8422) was provided by Japan Collection of Microorganisms, RIKEN BRC, which participates in the National BioResource Project of the MEXT, Japan. This work was supported in part by JSPS KAKENHI (Grant Nos. 25102008 and 24657113 to K.K.), by the Okazaki ORION project, and by the Nanotechnology Platform Project and the Targeted Proteins Research Program from the Ministry of Education, Culture, Sports, Science and Technology, Japan (to K.K.).

Appendix A. Supplementary data

Supplementary data associated with this article can be found, in the online version, at http://dx.doi.org/10.1016/j.bbrc.2014.09.114.

References

[1] K. Tanaka, The proteasome: overview of structure and functions, Proc. Jpn. Acad. Ser. B Phys. Biol. Sci. 85 (2009) 12–36.
[2] W. Baumeister, J. Walz, F. Zühl, E. Seemüller, The proteasome: paradigm of a self-compartmentalizing protease, Cell 92 (1998) 367–380.
[3] O. Coux, K. Tanaka, A.L. Goldberg, Structure and functions of the 20S and 26S proteasomes, Annu. Rev. Biochem. 65 (1996) 801–847.
[4] J. Löwe, D. Stock, B. Jap, P. Zwickl, W. Baumeister, R. Huber, Crystal structure of the 20S proteasome from the archaeon *T. acidophilum* at 3.4 Å resolution, Science 268 (1995) 533–539.
[5] M. Unno, T. Mizushima, Y. Morimoto, Y. Tomisugi, K. Tanaka, N. Yasuoka, T. Tsukihara, The structure of the mammalian 20S proteasome at 2.75 Å resolution, Structure 10 (2002) 609–618.
[6] R. Beckwith, E. Estrin, E.J. Worden, A. Martin, Reconstitution of the 26S proteasome reveals functional asymmetries in its AAA+ unfoldase, Nat. Struct. Mol. Biol. 20 (2013) 1164–1172.
[7] D.M. Smith, S.C. Chang, S. Park, D. Finley, Y. Cheng, A.L. Goldberg, Docking of the proteasomal ATPases' carboxyl termini in the 20S proteasome's α ring opens the gate for substrate entry, Mol. Cell 27 (2007) 731–744.
[8] G.C. Lander, E. Estrin, M.E. Matyskiela, C. Bashore, E. Nogales, A. Martin, Complete subunit architecture of the proteasome regulatory particle, Nature 482 (2012) 186–191.
[9] K. Lasker, F. Förster, S. Bohn, T. Walzthoeni, E. Villa, P. Unverdorben, F. Beck, R. Aebersold, A. Sali, W. Baumeister, Molecular architecture of the 26S proteasome holocomplex determined by an integrative approach, Proc. Natl. Acad. Sci. U.S.A. 109 (2012) 1380–1387.
[10] P.C. da Fonseca, J. He, E.P. Morris, Molecular model of the human 26S proteasome, Mol. Cell 46 (2012) 54–66.
[11] E. Kish-Trier, C.P. Hill, Structural biology of the proteasome, Annu. Rev. Biophys. 42 (2013) 29–49.
[12] R.J. Tomko Jr., M. Hochstrasser, Molecular architecture and assembly of the eukaryotic proteasome, Annu. Rev. Biochem. 82 (2013) 415–445.
[13] Y. Nakamura, T. Umehara, A. Tanaka, M. Horikoshi, B. Padmanabhan, S. Yokoyama, Structural basis for the recognition between the regulatory particles Nas6 and Rpt3 of the yeast 26S proteasome, Biochem. Biophys. Res. Commun. 359 (2007) 503–509.
[14] S. Kim, Y. Saeki, K. Fukunaga, A. Suzuki, K. Takagi, T. Yamane, K. Tanaka, T. Mizushima, K. Kato, Crystal structure of yeast rpn14, a chaperone of the 19S regulatory particle of the proteasome, J. Biol. Chem. 285 (2010) 15159–15166.
[15] K. Takagi, S. Kim, H. Yukii, M. Ueno, R. Morishita, Y. Endo, K. Kato, K. Tanaka, Y. Saeki, T. Mizushima, Structural basis for specific recognition of Rpt1p, an ATPase subunit of 26S proteasome, by proteasome-dedicated chaperone Hsm3p, J. Biol. Chem. 287 (2012) 12172–12182.
[16] M.B. Barrault, N. Richet, C. Godard, B. Murciano, B. Le Tallec, E. Rousseau, P. Legrand, J.B. Charbonnier, M.H. Le Du, R. Guerois, F. Ochsenbein, A. Peyroche, Dual functions of the Hsm3 protein in chaperoning and scaffolding regulatory particle subunits during the proteasome assembly, Proc. Natl. Acad. Sci. U.S.A. 109 (2012) E1001–E1010.
[17] C.R. Singh, S. Lovell, N. Mehzabeen, W.Q. Chowdhury, E.S. Geanes, K.P. Battaile, J. Roelofs, 1.15 Å resolution structure of the proteasome-assembly chaperone Nas2 PDZ domain, Acta Crystallogr. F Struct. Biol. Commun. 70 (2014) 418–423.
[18] T. Satoh, Y. Saeki, T. Hiromoto, Y.H. Wang, Y. Uekusa, H. Yagi, H. Yoshihara, M. Yagi-Utsumi, T. Mizushima, K. Tanaka, K. Kato, Structural basis for proteasome formation controlled by an assembly chaperone Nas2, Structure 22 (2014) 731–743.
[19] H. Yashiroda, T. Mizushima, K. Okamoto, T. Kameyama, H. Hayashi, T. Kishimoto, S. Niwa, M. Kasahara, E. Kurimoto, E. Sakata, K. Takagi, A. Suzuki, Y. Hirano, S. Murata, K. Kato, T. Yamane, K. Tanaka, Crystal structure of a chaperone complex that contributes to the assembly of yeast 20S proteasomes, Nat. Struct. Mol. Biol. 15 (2008) 228–236.
[20] B.M. Stadtmueller, E. Kish-Trier, K. Ferrell, C.N. Petersen, H. Robinson, D.G. Myszka, D.M. Eckert, T. Formosa, C.P. Hill, Structure of a proteasome Pba1–Pba2 complex: implications for proteasome assembly, activation, and biological function, J. Biol. Chem. 287 (2012) 37371–37382.
[21] A.R. Kusmierczyk, M.J. Kunjappu, R.Y. Kim, M. Hochstrasser, A conserved 20S proteasome assembly factor requires a C-terminal HbYX motif for proteasomal precursor binding, Nat. Struct. Mol. Biol. 18 (2011) 622–629.
[22] K. Kumoi, T. Satoh, K. Murata, T. Hiromoto, T. Mizushima, Y. Kamiya, M. Noda, S. Uchiyama, H. Yagi, K. Kato, An archaeal homolog of proteasome assembly factor functions as a proteasome activator, PLoS One 8 (2013) e60294.
[23] Z. Otwinowski, W. Minor, Processing of X-ray diffraction data collected in oscillation mode, Methods Enzymol. 276 (1997) 307–326.
[24] S.R. Ness, R.A. de Graaff, J.P. Abrahams, N.S. Pannu, CRANK: new methods for automated macromolecular crystal structure solution, Structure 12 (2004) 1753–1761.
[25] K. Cowtan, An automated procedure for phase improvement by density modification, Joint CCP4 ESF-EACBM Newslett. Protein Crystallogr. 31 (1994) 34–38.
[26] G. Langer, S.X. Cohen, V.S. Lamzin, A. Perrakis, Automated macromolecular model building for X-ray crystallography using ARP/wARP version 7, Nat. Protoc. 3 (2008) 1171–1179.
[27] P. Emsley, B. Lohkamp, W.G. Scott, K. Cowtan, Features and development of Coot, Acta Crystallogr. D Biol. Crystallogr. 66 (2010) 486–501.
[28] G.N. Murshudov, A.A. Vagin, E.J. Dodson, Refinement of macromolecular structures by the maximum-likelihood method, Acta Crystallogr. D Biol. Crystallogr. 53 (1997) 240–255.
[29] S.C. Lovell, I.W. Davis, W.B. Arendall 3rd, P.I. de Bakker, J.M. Word, M.G. Prisant, J.S. Richardson, D.C. Richardson, Structure validation by Cα geometry: φ, ψ and Cβ deviation, Proteins 50 (2003) 437–450.
[30] A.L. Menon, F.L. Poole 2nd, A. Cvetkovic, S.A. Trauger, E. Kalisiak, J.W. Scott, S. Shanmukh, J. Praissman, F.E. Jenney Jr., W.R. Wikoff, J.V. Apon, G. Siuzdak, M.W. Adams, Novel multiprotein complexes identified in the hyperthermophilic archaeon *Pyrococcus furiosus* by non-denaturing fractionation of the native proteome, Mol. Cell. Proteomics 8 (2009) 735–751.